2004 International ANSYS Conference

Pittsburg, PA, May 24-26, 2004

3D Engineered Fiberboard: Finite Element Analysis of a New Building Product

John F. Hunt, P.E.

USDA Forest Service, Forest Products Laboratory

Abstract

This paper presents finite element analyses that are being used to analyze and estimate the structural performance of a new product called 3D engineered fiberboard in bending and flat-wise compression applications. A 3x3x2 split-plot experimental design was used to vary geometry configurations to determine their effect on performance properties. The models are based on a simple corrugated geometry. Both 2D and 3D analyses were used for the compression and bending simulations, respectively. The material properties used in this analysis were obtained from tensile tests of flat panels made from processed tree top material. These finite element models have provided the ability to manipulate design configurations to estimate performance. The results show slight variations in core geometry produces significantly different and non-intuitive deformation and buckling results. These results also demonstrate the need for using a finite element approach to analyze non-symmetric non-uniform geometries because what seems to be good simplifying assumptions using engineering equations but may lead to significant errors in determining deformation responses or needed stiffness in a design.

Introduction

In many forests across the United States high fuel loadings due to a variety of reasons have contributed to our recent forest fire problems. Many fire-prone timber stands are generally far from traditional timber markets or the timber is not economically valuable enough to cover the costs of removal. In the western states, much of the fuel load can be characterized as small diameter or thinning material that has little or no commercial value. In a logging or thinning operation much of this low value material (Figure 1 and Figure 2) is either left standing or is felled and left on the ground, chipped, or burned because most North American mills are not equipped to handle it and it is an increasing fire hazard as it dries. To help address this problem, the USDA Forest Products Laboratory has developed a process to produce three-dimensional structural fiberboard products that can utilize a wide range of lignocellulosic fibers contained in the forest undergrowth, underutilized timber, and agro-biomass. A viable commercial process will encourage the private sector to remove these dangerous fuels and minimize federal costs for fire mitigation. The newly developed product is an engineered wet-pulp-molded structural material formed and hot-pressed between rigid molds with or without supplemental adhesive. When the structural core is bonded to exterior skins three-dimensional sandwich panels called '3D Engineered Fiberboard' are formed that exhibit a high level of strength and stiffness with significantly less material. The proposed fiberboard forming technology has a number of promising uses in construction, furniture and packaging applications.

A research project currently funded under the USDA Forest Service "National Fire Plan" [Hunt and Winandy, 2002b] is working on developing ways to use this material. The project's scope is to develop a viable value-added three-dimensional (3D) engineered structural fiberboard. The USDA Forest Products Laboratory has been working on processing methods to reduce various types of lignocellulosic material into a bondable fibrous mixture that can be formed and dried in a prescribed way to achieve a 3D engineered fiberboard with predictable performance properties. The proposed technology has promising uses in the construction of pallets, bulk bins, heavy duty boxes, shipping containers, packaging supports, wall panels, roof panels, cement forms, partitions, displays, reels, desks, caskets, shelves, tables, and doors. The size of these potential markets is enormous. For example, according to 1996 statistics published in the Annual Survey of Manufacturers [ASM, 1996], the pallet industry has annual sales in the U.S. of over $3 billion, wood office furniture is a $2.4 billion market, wood partitions and fixtures are a $3.7 billion market, and wood doors account for $2.2 billion of the total door market. The challenge is to develop methods to take low-value material and transform it into a value-added material that would have advantages over commodity wood products.

To appropriately use this material or other fibrous material for value-added 3D structural products requires that the engineered structure be designed based on the material properties and geometrical considerations. If the design were similar to common geometrical cases, i.e. I-beam, a strength-of-materials approach would be an easy and useful first approximation (Figure 3). However, structural optimization or processing limitations may require the design to deviate from the "simplified" cases, which then complicates the design process. To address the complex nature of the material and for optimizing the shape for a given performance, a finite element analysis (FEA) approach is necessary. Similar work has been done with corrugated paper box structures [Gilchrist et.al., 1999; Urbanik and Saliklis, 2003]. Corrugated paper structural models are constrained by: highly directional paper properties, predescribed corrugated flute geometry, and packaging like loading conditions. There are no known investigations of 3D engineered structural panels from paper like fibers. The structural panel analyses in this report and others to follow differ in panel size, loading conditions, performance needs, 3D geometry variations, 3D forming considerations, 3D fiber alignment considerations, higher density and higher strength components, thicker components, etc. This paper describes the initial investigation for this type of structure. Basic engineering mechanics equations and FEA methods were used to analyze a simplified 3D structural panel. Two standard tests, bending and flat-wise compression, were used to model and estimate deformation and load carrying capacity for a corrugated structural sandwich panel having different variations of the core geometry. The results from these models will then be used to compare actual test data from formed and pressed 3D structural panels.

Material Properties

The material properties used for this analysis were obtained from fibrous wood material obtained from small diameter treetops [Hunt and Winandy, 2002a]. The fibers were wet-formed into a flat mat and press-dried into flat panels 2.54 mm (0.1 in) thick. Drying under heat and pressure fibers bond together without adhesives or additives. The flat panels were evaluated for their tensile and bending properties [Hunt and Supan, 2004] following American Society for Testing and Materials (ASTM) Standard D-1037 [ASTM, 1996] test method. The material properties obtained from the flat panel tests [Hunt and Supan, 2004] were used for inputs for the finite element analysis. The strength and modulus of elasticity (MOE) values were 44 MPa (6416 PSI) and 6.1 GPa (0.89 MPSI), respectively. These wood fiber composite materials can be described as a short-fiber planer composite material with the predominant fiber orientation being randomly distributed in-plane. The in-plane properties are isotropic and properties normal to the fiberboard are significantly less in both strength and stiffness. Normal flat-panel properties have not been fully characterized. Plans are to measure the orthotropic constitutive properties and input those into the model at a later date.

For these analyses, the material properties are assumed isotropic and linear elastic with a Poisson's ratio of 0.3. Tensile and compression strengths and moduli values are assumed the same based on similar tension-to-compression strength comparisons for wet-formed hardboard [Suchsland and Woodson, 1986].

Modeling

To study the performance characteristics of the 3D engineered fiberboard, two models, a 2D and a 3D, were developed using FEA software developed by ANSYS and their ANSYS Parametric Design Language (APDL) programming language. Both analyzed the same cross-sectional geometry, but the 3D model analyzed the bending performance and the 2D model analyzed flat-wise compression performance. A 3x3x2 experimental design (Table 1) was used to study the effects of several input parameters on the structural performance, they were: 1. core rib angle α; 2. core rib thickness $\boldsymbol{t}$; 3. rib spacing $\boldsymbol{w}$ (Figure 4) and 4. pattern width (Figure 5). The cross-sectional geometry can be best described as a modified corrugated geometry having a constant thickness with straight rib and flange sections and constant radius transitions. The inside rib radius dimension was 1.6 mm (0.0625 inches). A radius rib transition (Figure 4) was chosen for the model to better simulate the actual design of the 3D engineered core rather than a sharp angle transition (Figure 6) that was used for initial engineering calculations. For both models, contact element pairs were placed between all the radius points of contact. The cross-sectional properties such as area and MOI were determined using ANSYS's beam section routine. Both models were solved using large-displacement transient solution option provided in ANSYS.

3D Bending Model

The 3D bending model for the beam was developed to simulate the ASTM C 393 standard [ASTM C 393] test used for evaluating structural sandwich constructions. The model included the rounded mid-point load applicator and reaction load point. The beam's cross-section was generated in the APDL program, then extruded three times to provide three distinct sections on the beam so different size elements could be assigned to each. The first cross-sectional extrusion was 50.8 mm (2.0 inch) and located over the reaction support. The second extrusion was 203 mm (8.0 inch) and was used for the mid-section. The third extrusion was 25.4 mm (1.0 inch) and was used for under the load (Figure 7). The total beam length was determined based on being able to form similar beams for testing using the fiber forming capabilities at FPL. Forming and pressing molds have been designed to specifically test and evaluate the 3D engineered fiberboard concept (Figure 8). Due to symmetry, only half of the beam and half of the pattern were modeled. Geometrical symmetry boundary conditions were defined at the beam's mid-point cross-sectional area and on the areas along both sides of the beam. The curved mid-point load surface and reaction surface were rigid surfaces with contact point pairs between the surfaces at both locations. Solid187, 10-node tetrahedron, was the global element type used for this model. Additional contact pairs were used between the curved core areas and the inside flange areas. To keep element sizes uniform from one model variation to the next, the element size was based on a ratio of rib thickness or face thickness and were defined within the ANSYS APDL program.

The applied beam load ***Po*** was estimated by rearranging the modulus of rupture (MOR) equation for a simply supported beam (Equation 1). For this study, the maximum tensile stress value from the flat panel tests [Hunt and Supan, 2004] was used as the failure stress, σ_{cr}, or MOR of the outer portion of the beam.

$$\sigma_{cr} = \frac{Md}{I_b} = \frac{(P_o/2)(L/2)d}{I_b} \quad \rightarrow \text{Rearranged} \rightarrow \quad P_o = \frac{I_b \sigma_{cr}}{(L/4)d} \quad \text{-------------------------------------} \quad 1$$

Where $\boldsymbol{\sigma_{cr}}$ is the maximum stress at failure = 44 MPa; ***M*** is maximum moment; ***d*** is the distance from the neutral axis to the top or bottom surface = 0.019 m (0.75 in); $\boldsymbol{P_o}$ is the total beam load; ***L*** is total span length, ***L*** = 0.51 m (20 in); $\boldsymbol{I_b}$ is the area moment of inertia for the beam's cross-section.

Using the design parameters as listed in Table 1, the equation predicts that the beam failure load would vary from 51 to 58 kN/m-width (292 to 334 lbs/in-width). For the FEA model, an applied full beam load of 52.5 kN/m-width (300 lb/in-width) was used for $\boldsymbol{P_o}$ or ½ that value was applied for the ½ beam model ($\boldsymbol{P_o/2}$) because of symmetry. The number of elements for these models was around 50,000 and increased as the pattern width increased.

2D Flat-Wise Compression Model

When using solid wood panel products there is not much concern for compression failure because for most applications the solid wood structure does not usually exhibit crushing. However, for a 3D engineered fiberboard structural sandwich panel, compression effects must be considered because up to 2/3^{rds} of the material could be removed from the core. The 2D flat-wise compression model was developed to simulate the ASTM C 365 standard [ASTM C 365] test including a solid steel load applicator. Symmetry boundary conditions were defined on the beam's sides including those on the load applicator. ANSYS element type plane183, an 8-node quad, was used as the global element type for this model. Similar to the 3D model, the element sizes were kept uniform from one model variation to the next. The element sizes were defined in the APDL program as ratios of rib thickness. Element sizes were also selected for the contact pair lines, using the ANSYS spacing ratio option either greater or less than 1.0 to generate skewed elements with the smaller elements closest to the contact point and increasing away from the contact point. A maximum pressure of 4.1 MN/m per unit depth (600 lbs/in per unit depth) was applied to the top line on the load applicator and was used to determine rib failure behavior, buckling or compression. This load was obtained from initial estimates for determining buckling of the core rib. The number of elements for these models was approximately 2,000 and varied slightly depending on the core geometry parameters.

Results & Discussion

3D Bending Model

With the large displacement option applied all data was saved at every 5 sub steps until full load was applied. Beam deflections for all the variations are listed in Table 2. For each pattern width, deflection data is based on equal load per unit width of beam, 52.5 kN/m (150 lb/in), which results in different total beam loads of 2.67 kN (300 lbs) and 4.0 kN (450 lbs) for the 50.8 mm (2.0 inch) and 76.2 mm (3.0 inch) wide pattern widths, respectively. The deflections in the first column for each pattern width are based on equation 2. This equation assumes no deflection due to shear or core deformation. Comparing the values, they predict both decreasing deflections due to increasing rib thickness and increasing rib angle. Both these two parameters increase MOI, which decreases deflection, as expected.

$$y = \frac{P_o L^3}{48EI} \qquad \text{----------} \qquad 2$$

Where P_o is the beam load; L is the beam length; E is the modulus of elasticity; and I is the area moment of inertia.

Because the beam's span-to-depth ratio is only 13.3, less than the test standard of 24, and the thin rib section will cause higher than normal shear stress resulting in shear deflection, which should be included in the analysis. For conventional I-beams there is a form factor, equation 3, which is used in equation 4 to calculate shear deflection (y_s) for mid-point loading [Young, 1989]. While our geometry is not exactly a perfect I-beam, its shape is a close approximation (Figure 4 and Figure 6).

$$F = \left[1 + \frac{3(D_2^2 - D_1^2)D_1}{2D_2^3}\left(\frac{w}{a} - 1\right)\right]\frac{4D_2^2}{10r^2} \qquad \text{----------} \qquad 3$$

$$y_s = \frac{1}{4} F \frac{P_o L}{AG} \qquad \text{----------} \qquad 4$$

Where
D_1 = distance from the neutral axis to the nearest surface of the flange (***D_1 = h/2-t/2***)
D_2 = distance from the neutral axis to the extreme fiber (***D_2 = h/2***)
a = horizontal thickness of the web (***a = t/sinα***)
w = width of the flange (*w*)
r = radius of gyration of the section with respect to the neutral axis.
P_o = beam load
L = span length
A = cross-sectional area
G = modulus of rigidity (shear modulus) and is determined by the relationship ***G = E/(2(1+ν))***

The second column under each pattern width of Table 2 shows this additional effect of shear on the total deflection. The shear equation accounts for an additional 7% to 16% more deflection. The effect of shear deflection decreases with increasing rib thickness and increasing angle. As the rib thickness increases more material is available for distributing the shear load, thus shear deflection decreases. In a similar way, as the rib angle increases the total cross-sectional area (***A***) increases, which decreases the stress throughout the part, and thus decreases the shear deflection. These shear trends were expected.

The third column under each pattern width of Table 2 shows the deflection of the beam predicted by FEA. Deflection values were taken from the bottom of the beam. Deflection decreases with increasing rib thickness, as with the beam deflection equations 2 and 4. However, the decreasing deflections with decreasing rib angles are counter intuitive as they are opposite to the trend calculated from these standard beam equations. FEA predicts the stiffest beam for this study is with a rib angle of 50° and not 90°, a rib thickness of 2.54 mm (0.1 inch), and a rib pattern of 50.8 mm (2.0 inches). The FEA deflection for this beam configuration, -4.75 mm (0.187 inch), is also the closest compared to the deflections from the beam equation that include shear, equation 4, deformation, -4.34 mm (0.171 inch), which only differs by 9%. All other deflections predicted by FEA are significantly more than those predicted from the engineering equations. To verify these evaluations another FEA run was conducted for the 2.54 mm (0.10 inch) rib thickness, 50.8 mm (2.0 inch) pattern width, and 90-degree rib angle using twice the number of elements. The resulting deformation for the second run was –7.34 mm compared with –7.37 mm for the initial run, a change of only 0.2%, so the initial analyses provided reasonable results.

The bottom flange longitudinal stress values, MOR, calculated from equation 1 and obtained from the FEA 50.8 mm (2.0 inch) pattern width model are shown in Figure 9. (Similar results were obtained for equation 1 and FEA 76.8 mm (3.0 inch) pattern width, but are not shown for clarity of the figure.) The maximum stress value decreases with the equation 1 as rib angle increases and as rib thickness increases. The FEA evaluation also shows decreasing stress as rib thickness increases, however, as rib angle increases stress also increases, opposite of the standard beam equation 1. It is fairly intuitive that as the rib thickness increases more material is placed into the rib section where load can be shared across more material thus reducing the stress level on the outer parts of the flange. However, it is not obvious how the interaction of geometry of the rib for the curved radius sections and angled rib section influence the stress response. Further investigation to fully understand all states of stress during bending of an engineered core needs to be done. In Figure 9, a line at 44.2 MPa (6416 PSI) was placed to indicate maximum failure stress of the flanges, above this value the flanges would fail in tension or compression. Several configurations cross this line indicating failure would occur at those conditions represented above that line at the given beam load of 52.5 kN/m (300 lbs/in).

From this FEA bending evaluation, for the given geometry and material properties, where maximum bending strength and/or minimum deformation is needed, then a geometry with ribs oriented at 50 degrees should be specified. However, a more thorough analysis should be conducted to determine at what rib angle on either side of 50 degrees maximum stiffness is predicted to occur. This comparison shows that potential errors could occur if "simplifying" assumptions were made and the only engineering equations used for the design. The engineering equations taken from engineering handbooks were developed for uniform and symmetric I-beams. They do not account for localized buckling nor do they account for core displacement at the core radius areas. The finite element approach may be the only way to accurately predict stiffness for non-standard 3D engineered beams. To fully understand the increased deflection due to buckling and core deformation predicted by FEA, further analysis of the states-of-stress needs to be studied as well as true comparisons from actual beam tests. This analysis and comparison is beyond the scope of this paper, but is currently being studied and will be reported in later publications.

2D Flat-Wise Compression Model

For many wood composites, bending strength, MOR, and deformation are the two main test values used for defining performance. The bending test provides engineers with estimated performance characteristics for many load conditions, however, there are still others where loads normal to the panel are the dominant performance requirement and the response to these loads must also be determined.

For ribbed structures, two common modes of failure are rib compression or rib buckling when loading normal to the panel. Depending on the geometry and elastic properties, one or the other failure mechanisms may occur. For compression failure, the criterion is based only on the maximum compressive strength properties parallel to the rib, ($\sigma_{cr} = P_{cr\text{-}c}$/area). Rearranging this equation and using the estimated maximum compressive stress value for the material, it is possible to estimate the maximum critical load carrying ($P_{cr\text{-}c}$) capacity per rib per unit depth (Equation 5). This $P_{cr\text{-}c}$ acts parallel to the rib, but for designs with ribs oriented other than 90 degrees it is necessary to know the maximum normal applied load (P_o) (Figure 6). P_o can be calculated from equation 6 where the normal applied load decreases as the rib angle (α) decreases, or in other words the panel load carrying capacity decreases as the rib angle decreases.

$$P_{cr-c} = \sigma_{cr}(t*1) \quad \text{-----} \quad 5$$

Where ***t*** is rib thickness and ***1*** is the unit depth.

$$P_o = P_{cr-c}\cos(90-\alpha) \quad \text{-----} \quad 6$$

The compression failure criterion does not take into consideration any geometry issues of the ribs. If the rib length to thickness (l_{cr}:t) ratio is too high, then the ribs can act as miniature columns and fail by buckling far below the calculated compression failure stress. Equation 7 is used to estimate the critical load (P_{cr-b}) when buckling failure would occur [Avallone and Baumeister, 1987].

$$P_{cr-b} = \frac{n\pi^2 EI_r}{l_{cr}^2} \quad \text{-----} \quad 7$$

Where P_{cr-b} is the critical buckling load; n is the column end condition factor; n = 4 for both ends fixed; E is the modulus of elasticity; I_r is the area moment of inertia for the ribs' cross-section; and l_{cr} is the rib column length parallel with the rib angle.

If buckling does not occur then the ribs compress under a known load, and if the load is not sufficient to cause compression failure then there is another engineering assessment for design, which is to determine if flat-wise deformation is within acceptable limits. Using the modulus of elasticity equation relationship of stress/strain, the basic terms can be rearranged to determine the change in thickness normal to the faces (Δl_o) (Figure 6) due to compressive loads using equation 8.

$$\Delta l_o = \frac{l_o \frac{P_{cr}}{t*1}}{E} \quad \text{-----} \quad 8$$

Where l_o is the original core rib height; t is the rib thickness; E is the modulus of elasticity; P_{cr} is the critical load parallel with the rib angle.

For the FEA analyses, the rib thickness-to-length ratio chosen fell near the cross over between buckling and compression failure criteria where failure would depend on the rib angle and rib thickness. Figure 10 shows predicted buckling or compression failure values for a rib thickness of 1.27 mm (0.50 inch). Failure is predicted to occur at the lower of the two values. The failure mode crosses over at just below 80 degrees, where buckling is predicted to occur for rib angles less than 80 degrees and compression failure is predicted to occur at or above 80 degrees. These predicted values are from a straight ribbed core I-beam (Figure 6) compared to the radius-ribbed core (Figure 4) used in the FEA analyses. The straight ribbed core I-beam represents a simplified geometry approach to estimate compression performance of an actual model (Figure 8) that is being used to form 3D engineered fiberboard.

The FEA 2D model was used to estimate flat-wise compression performance of the ribbed structures for different load applications. A 4.1 MN/m per m-depth (600 lbs/in per in-depth) compressive pressure was applied across a 25.4 mm (1.0 inch) wide steel plate. Because the geometry being analyzed by FEA is made of a core with two radius sections and a straight rib section it was of interest to separate the effects of these two on the total deformation. Additional rib angles of 60° and 80° were added to the analysis to better understand what effect rib angle and the rib radius have on total deformation. Deformation values were evaluated for one rib only over a per-unit-area rather than over a particular pattern width. Total load carrying capacity for the two pattern widths would be calculated from the number of ribs per unit area. Comparisons with the FEA data were also made with a simplified straight ribbed I-beam. All FEA models were solved using the large displacement analysis option. Deformation and rib stress values were recorded at every load sub step.

Compression deformation vs. load results for all the 1.27 mm (0.05 inch) rib configurations (Figure 11) results show that rib buckling occurred before the full load was ever reached. Maximum deformation occurred with the 90-degree rib configuration. The minimum deformation or stiffer response was achieved with the 60-degree rib configuration, prior to buckling. The buckling load and resulting deformation estimated from equations 7 and 8, also plotted, are shown to be significantly different than those predicted by FEA. These equations predict that for the 50-degree rib orientation buckling should occur at approximately 25 KN/m-depth (144 lbs/in-depth), with 0.12 mm (0.005 inch) deformation. This is significantly different that FEA's results which are approximately 33 kN/m-depth (190 lbs/in-depth) load with a 0.39 mm (0.016 inch) deformation. For the 70-degree rib, equation 7 predicts a buckling load of 49 kN/m-depth (279 lbs/in-depth) which is about the same as FEA's but, the predicted deformation, 0.19 mm (0.007 inches), is about ½ that obtained from the FEA model. Then for the 90-degree rib orientation, equation 7 predicts failure to occur near 60 kN/m-depth (340 lbs/in-depth), far greater than what FEA predicted at a deformation, 0.19 mm (0.007 inches), which is far less than that predicted by FEA. Both deformation and buckling load differences can be attributed to geometry consideration in the radius sections of the core. Deformation plotted for just the straight section of the rib (Figure 12) shows that the straight rib deforms similarly to those predicted by equation 8, as would be expected. The additional deformation for the core with radius rib sections then, must come from bending and deformation of those radius sections. A bending moment resulting from the rib load, shown as $\boldsymbol{P_{cr}}$ in Figure 6, causes a "cantilever-beam" deformation. As the rib angle increases, the length of the moment arm increases, thus resulting in more "bending" deformation in the radius section. For the 90-degree rib orientation, the radius section deformation is greater than for the 50-degree rib, Figure 13. It is interesting to note then, that with these complex interacting deformation effects the FEA predicts minimum total deformation for the 1.27 mm (0.05 inch) thick ribs is for a rib angle somewhere between 50 and 70 degrees (Figure 11) and not at 90 degrees as one might intuitively expect. Equation 7 predicts buckling load should increase as the rib length decreases and as the MOI increases, which are at a minimum and maximum at 90 degrees, respectively.

A similar FEA analysis was done for the other two rib thicknesses, 1.90 mm and 2.54 mm, resulting in similar trends except deformation results were linear (no evidence of buckling) for the total deformation (Figure 14) and for both the straight and radius core sections. The maximum load and corresponding deformation were determined by interpolating stress values between load steps in order to determine when maximum compressive stress occurs parallel to the rib. Connecting these maximum load points at each rib angle shows the affects of rib angle on deformation and maximum load. A core with a 90-degree rib carries the maximum load, but it also has the maximum deformation. The stiffest core would have a rib angle somewhere around 70 degrees with average deformation. Failure loads increase with increasing rib angle, but deformation is non-linear. Loads calculated from equations 5 and 6 correlate well with the failure loads obtained by interpolation from FEA.

Figure 15 shows a comparison of all the configurations at a non-buckling load of 37 kN/(m-depth) (210 lbs/in-depth). This figure shows the trends of how geometry affects performance. For example, the 2.54 mm (0.10 inch) thick rib with an angle slightly less than 70 degrees yields the minimum deformation or maximum stiffness. As rib thickness decreases from 2.54 mm to 1.27 mm (0.10 inch to 0.05 inch) there is a shift toward smaller rib angles to obtain maximum core stiffness. The deformation values for the straight section of the rib indicate that a shift toward 90 degrees would occur as rib thickness increases. Deformation and load values for the FEA straight rib section approach the values calculated from the load and deformation equations 5 and 8, which is what would be expected.

To verify these predicted responses fiber-based structural panels will be formed and tested to compare actual panel results with the model. Results from the actual tests and those from these models will be compared and improvements to the FEA model made were needed. Future work is also planned to improve these models including the use of non-linear visco-elastic orthotropic properties and an improved description of non-uniform distribution of the fiber-based material properties. The goal is to produce a more realistic prediction of 3D fiberboard that can then be truly called engineered.

Conclusions and Comments

Two FEA models, a 2D and a 3D, are presented that model ASTM standard bending and flat-wise compression tests. These models can be used to predict potential performance behavior for a 3D engineered wood fiber composite. While these current models assume linear elastic and isotropic material properties, general trends and characteristics can be determined to help optimize future designs. These analyses show how rib angle, rib radius, and rib thickness have a significant affect on total performance and conflicting interactions can produce non-intuitive results.

Significant differences were evident when the FEA estimated values for maximum flange stress and beam deformation were compared with those obtained from the beam equations 2 and 4. A finite element method can handle conflicting interactions and should be used when even small variations from standard geometrical modeling occur. Further analyses of the states of stress will be studied.

The 2D flat-wise compression model only considers the load per rib per unit depth. The number of ribs per unit width of a panel will also change load-carrying performance. This is a linear relationship where doubling or tripling the ribs per unit width will double or triple the normal load carrying capability or reduce by half or a third the deformation at a given load. The number of ribs per unit width has practical upper and lower limits based on fiber forming characteristics. Both forming and geometrical processing issues need to be considered simultaneously as future analyses are conducted. For example, a 90-degree rib is easy to describe geometrically and calculate the loads based on the angles and material properties, it may be difficult to fabricate in the forming and pressing process. As the rib angle decreases, it is easier to consolidate fibers into ribs using a conventional hot pressing and forming molds. This is important to remember when balancing the performance requirements with practical fiber forming characteristics and pressing methods. A reduced angle may be necessary for optimum fiber processing, which may then require a thicker rib or stiffer material to achieve the desired load carrying performance needs. Depending on the design, a thicker rib or stiffer material may change the failure mechanism from buckling to compression allowing the rib to carry even higher loads. Determining the optimum number of ribs or optimum forming angle for a specific application is outside the scope of this paper. The intent was to show the potential of 3D engineered fiberboard and the need for FEA as an analysis tool to determine the performance parameters.

This analysis assumed uniform properties for the along entire fiberboard core geometry, however this is many times difficult to achieve even with the best fiber forming technologies, so provisions should be made in the next model to include properties variations within the geometry. Non-uniform fiber forming creates non-uniform fiberboard density, which influences MOE. Non-uniform modulus may be a design feature or a design flaw depending on the final performance needs. Determining the influence of density along the length of the core is also outside the scope of this paper. This and the other forming considerations will be developed in later publications.

These analyses also assume isotropic linear elastic behavior. As more information is obtained on the orthotropic properties it is possible that internal stresses in the core may cause failure significantly before it would be predicted by either the equations or by isotropic FEA modeling. By placing accurate parameters into the model will allow for more realistic predictions and designs for engineering 3D fiberboard. This will be developed and analyzed further and included in later publications.

References

ASM, Annual Survey of Manufactures, 1996, Statistics for Industry Groups and Industries, U.S. Department of Commerce, Economics and Statistics Administration, BUREAU OF THE CENSUS, M96(AS)–1

ASTM Standard C 365 (1988): Standard Test Methods for Flatwise Compressive Strength of Sandwich Cores: American Society for Testing and Materials, West Conshohocken, PA

ASTM Standard C 393 (1988): Standard Test Method for Flexural Properties of Flat Sandwich Constructions: American Society for Testing and Materials, West Conshohocken, PA

ASTM Standard D 1037 (1996): Evaluating the Properties of Wood-Base Fiber and Particle Panel Materials: American Society for Testing and Materials, West Conshohocken, PA

Avallone, E.A. and Baumeister III, T.. 1987. Mark's Standard Handbook of Mechanical Engineering 9th Edition, McGRAW-HILL, INC., New York, p.5-18.

Gilchrist, A.C., Suhling, J.C., and Urbanik. T.J.. 1999. Nonlinear Finite Element Modeling of Corrugated Board. AMD-Vol. 231/MD-Vol. 85. Mechanics of Cellulosic Materials. ASME 1999 pp101-106

Hunt, J.F. and Supan, K., 2004. Mechanical Properties for a Wet-Processed Fiberboard made from Small Diameter Lodgepole Pine Tree-Top Material., Submitted for publication in Forest Prod. J.

Hunt, J.F. and Winandy, J.E., 2002a. 3D Engineered Fiberboard: A New Structural Building Product, 6th European Panel Products Symposium. Oct. 9-11, 2002. Llandudno, Wales. pp106-117

Hunt, J.F. and Winandy, J.E., 2002b. Using wood-based structural products as forest management tools to improve forest health, sustainability and reduce forest fuels: A research program at the USDA Forest Service under the National Fire Plan. Proc. Of the 6th Pacific Rim Bio-Based Composite Symposium. Nov. 10-13, 2002, Portland, OR USA, Vol. 1 pp319-323

Suchsland, O. and Woodson, G.E.. 1986. Fiberboard Manufacturing Practices in the United States. USDA Forest Service, Agriculture Handbook No. 640.

Urbanik, T.J. and Saliklis, E.P., 2003. Finite Element Corroboration of buckling Phenomena. Wood and Fiber Science, 35(3), 2003, pp. 322-333

Young, W.C. 1989. Roark's Formulas for Stress and Strain, Sixth Edition. McGraw-Hill, Inc. New York, NY

Tables and Figures

Table 1 Study 3x3x2 design matrix for the engineering analysis.

3x3x2 design matrix		Pattern Width	
		50.8 mm (2.0 in)	**76.2 mm (3.0 in)**
Rib Angle	**50 degrees**	Rib Thickness 1.27 mm (0.05 in) 1.90 mm (0.075 in) 2.54 mm (0.1 in)	Rib Thickness 1.27 mm (0.05 in) 1.90 mm (0.075 in) 2.54 mm (0.1 in)
	70 degrees	Rib Thickness 1.27 mm (0.05 in) 1.90 mm (0.075 in) 2.54 mm (0.1 in)	Rib Thickness 1.27 mm (0.05 in) 1.90 mm (0.075 in) 2.54 mm (0.1 in)
	90 degrees	Rib Thickness 1.27 mm (0.05 in) 1.90 mm (0.075 in) 2.54 mm (0.1 in)	Rib Thickness 1.27 mm (0.05 in) 1.90 mm (0.075 in) 2.54 mm (0.1 in)

Table 2. Center point beam deflection obtained from the Euler beam equation without shear (wo/shear) and with the shear equation (w/shear), and FEA. The beam comparison between pattern widths is equal load per unit width of the beam, but not equal beam load. (The darkened cells are the closest predictive deformation match between the FEA and standard beam equations.)

Angle (Degrees)	Rib Thickness mm (inch)	Beam Deflection – mm (inch)					
		Pattern Width – Beam Load					
		50.8 mm (2.0 in) - 2.67 kN (300 lbs)			76.2 mm (3.0 in) - 4.0 kN (450 lbs)		
		wo/shear	w/shear	FEA	wo/shear	w/shear	FEA
50	**1.27 (0.05)**	-4.18 (-0.164)	-4.81 (-0.189)	-6.76 (-0.266)	-4.13 (-0.163)	-5.03 (-0.198)	-8.37 (-0.330)
	1.90 (0.075)	-4.09 (-0.161)	-4.52 (-0.178)	-5.46 (-0.215)	-4.02 (-0.158)	-4.64 (-0.183)	-6.88 (-0.271)
	2.54 (0.10)	**-4.02** (-0.158)	**-4.34** (-0.171)	**-4.75** (-0.187)	-3.93 (-0.155)	-4.40 (-0.173)	-6.01 (-0.237)
70	**1.27 (0.05)**	-4.04 (-0.159)	-4.78 (-0.188)	-7.96 (-0.313)	-4.04 (-0.159)	-5.12 (-0.202)	-9.07 (-0.357)
	1.90 (0.075)	-3.91 (-0.153)	-4.40 (-0.173)	-6.79 (-0.267)	-3.90 (-0.154)	-4.63 (-0.182)	-7.78 (-0.306)
	2.54 (0.10)	-3.80 (-0.149)	-4.17 (-0.164)	-6.08 (-0.239)	-3.80 (-0.150)	-4.34 (-0.171)	-7.01 (-0.276)
90	**1.27 (0.05)**	-3.94 (-0.155)	-4.70 (-0.185)	-8.61 (-0.339)	-3.96 (-0.156)	-5.09 (-0.200)	-9.54 (-0.376)
	1.90 (0.075)	-3.77 (-0.148)	-4.27 (-0.168)	-7.85 (-0.309)	-3.81 (-0.150)	-4.56 (-0.180)	-8.49 (-0.334)
	2.54 (0.10)	-3.65 (-0.144)	-4.03 (-0.159)	-7.37 (-0.290)	-3.69 (-0.145)	-4.25 (-0.167)	-7.89 (-0.311)

Figure 1 Forest thinnings after 10+ years showing minimal decomposition and very dry conditions.

Figure 2 After a logging operation cutting small-diameter trees (left) there is still a significant amount of tree-top material (right) available as a fiber resource.

Figure 3 Preliminary design of a uniaxial corrugated core made from fiberized fibers from small diameter tree tops.

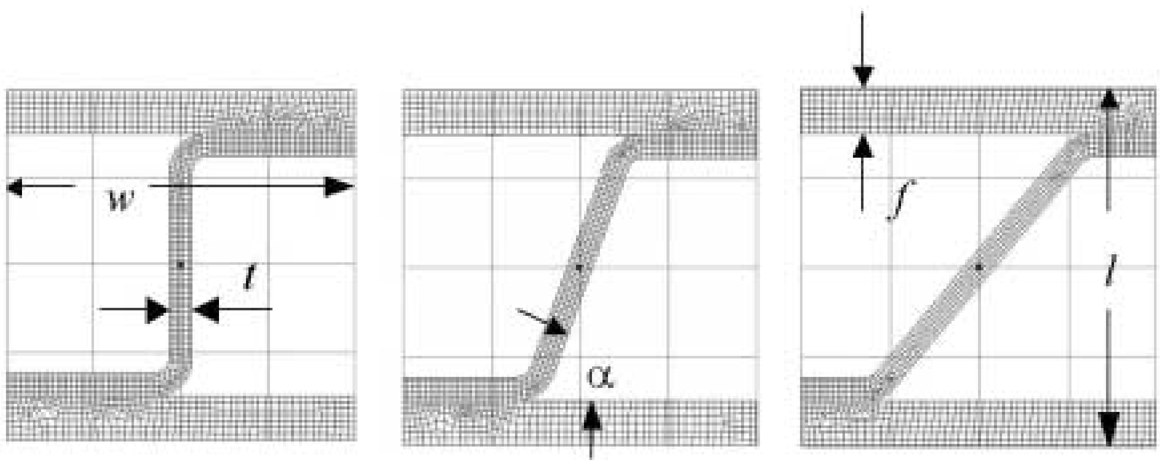

Figure 4 Geometrical input variables used for the FEA radius core finite element models showing three different angles, 90, 70, and 50 degrees.

50.8 mm (2.0 in) Pattern Width with 90 degree rib angle shown repeated 3 times.	
76.2 mm (3.0 in) Pattern Width with 90 degree rib angle shown repeated 2 times	

Figure 5 Two pattern widths (factor 1) used for this study are expanded here across a 15.2 cm (6.0 in) panel width for clarity of the drawings.

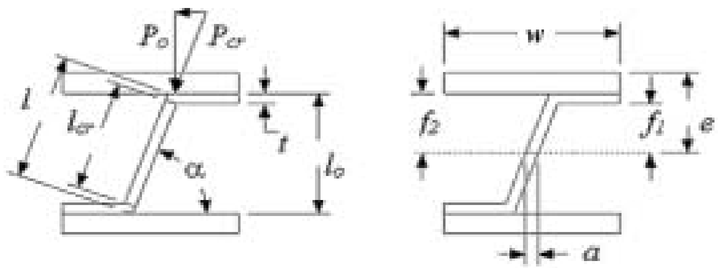

Figure 6 **Simplified geometry and input variables used for calculating buckling or compression equations to determine failure modes.**

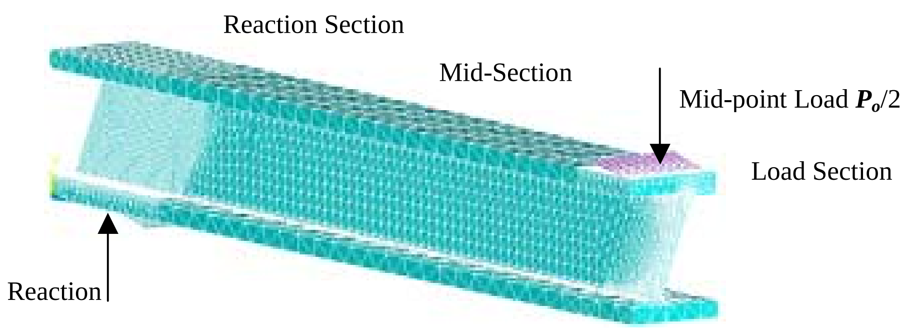

Figure 7 **3D beam configuration with the mid-point load shown at ½ symmetry at the mid-point and ½ the rib pattern. Core rib angle is 70 degrees, rib thickness is 1.27 mm, beam width is 25.4 mm. Model symmetry is along both sides of the beam and on the areas at the mid-point cross-section. Beam elements shown with varying element sizes for the three sections of the beam. Smaller elements were used under the load and reaction sections. The beam's rib angle shown is 70 degrees.**

Figure 8 **Aluminum mold designed to form 3D engineered fiberboard cores. Outside dimensions are 61 by 61 cm (24 by 24 inches).**

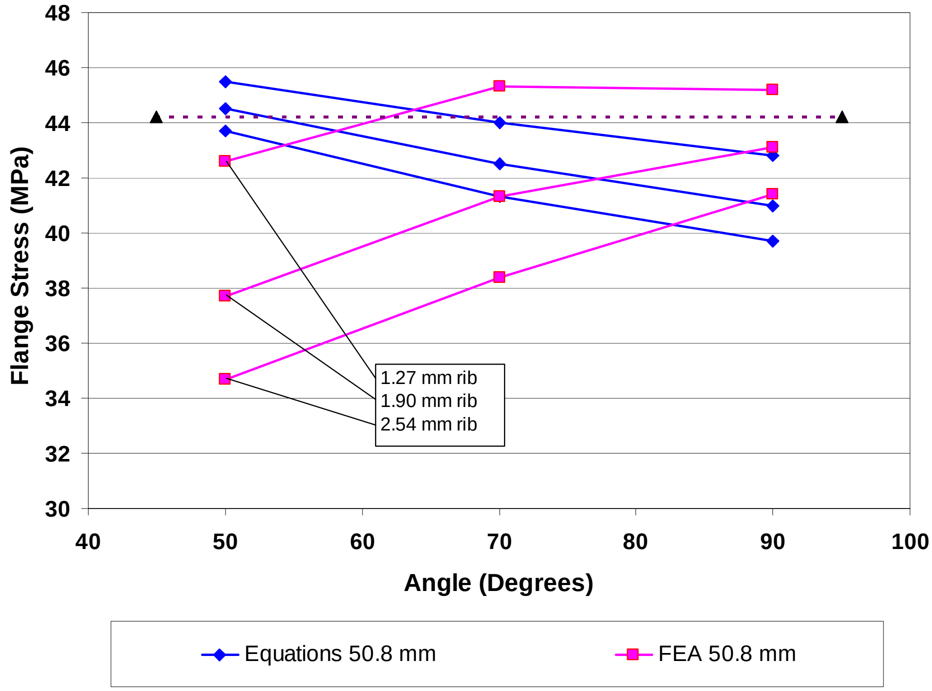

Figure 9. Bending flange stress vs. rib angle for both equation and FEA evaluation methods are evaluated at 52.5 kN/m for the 50.8 mm rib pattern. Each connected line in a series is a constant rib thickness. There are three constant rib thicknesses (lines) in a series having rib thicknesses of 1.27 mm, 1.90 mm, to 2.54 mm. The bottom line in each series is 2.54 mm thick rib. The straight dotted line at 44.2 MPa is the maximum failure tension and compression stress or modulus of rupture.

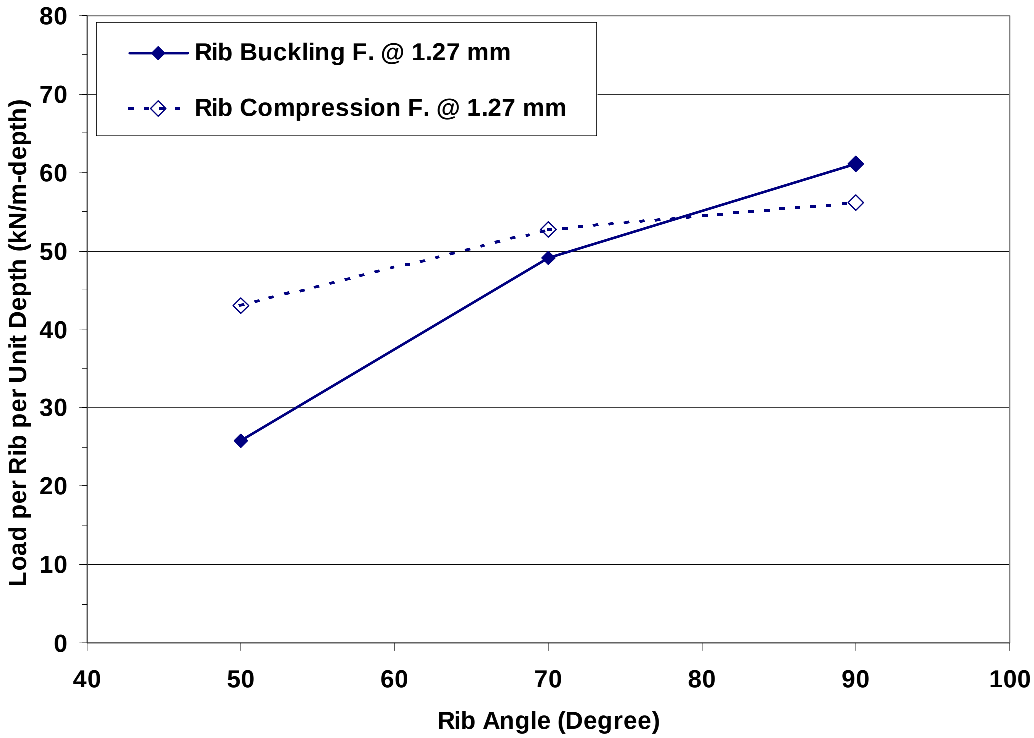

Calculations Based on Compression Strength = 44 MPa; MOE = 6.1 GPa

Figure 10 **Predicted rib buckling and compression failure for 1.27 mm rib thickness based on engineering buckling and compression equations. Failure is predicted to occur at the lower of the two calculated values at the corresponding rib angle.**

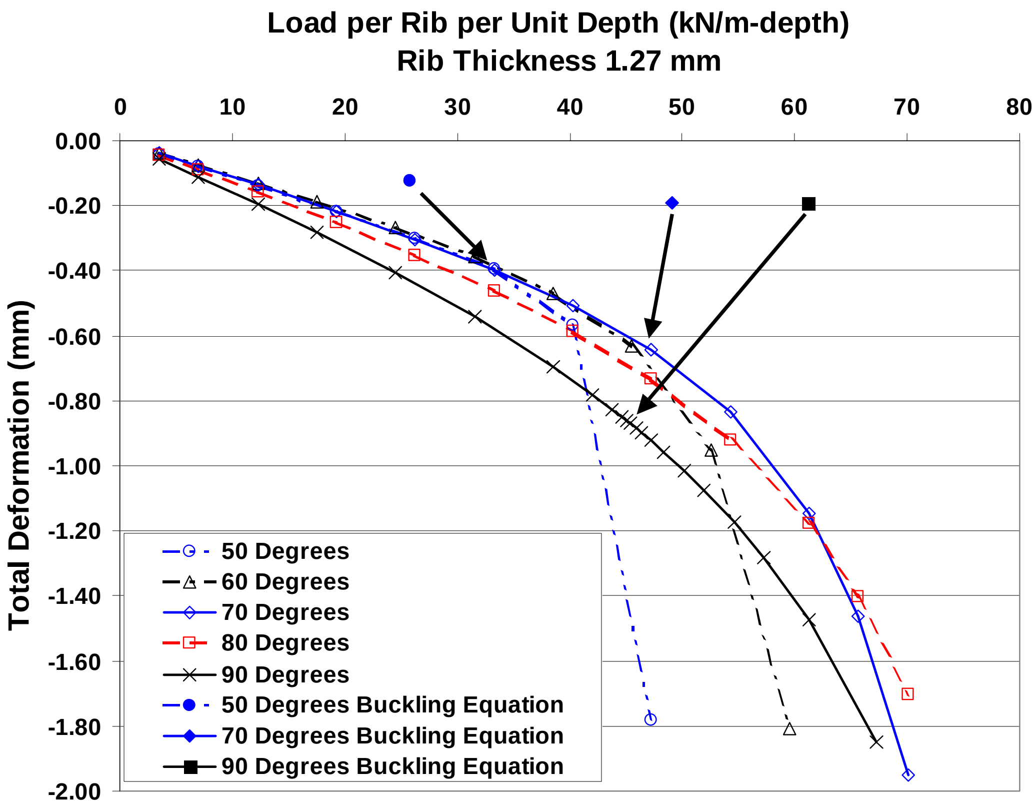

Figure 11 Total flat-wise compression for the 3D engineered fiberboard with a rib thickness of 1.27 mm. Buckling is evident based on the departure from a linear deformation curve. Results from the buckling equation are also plotted with corresponding point to approximate values where FEA predicts buckling.

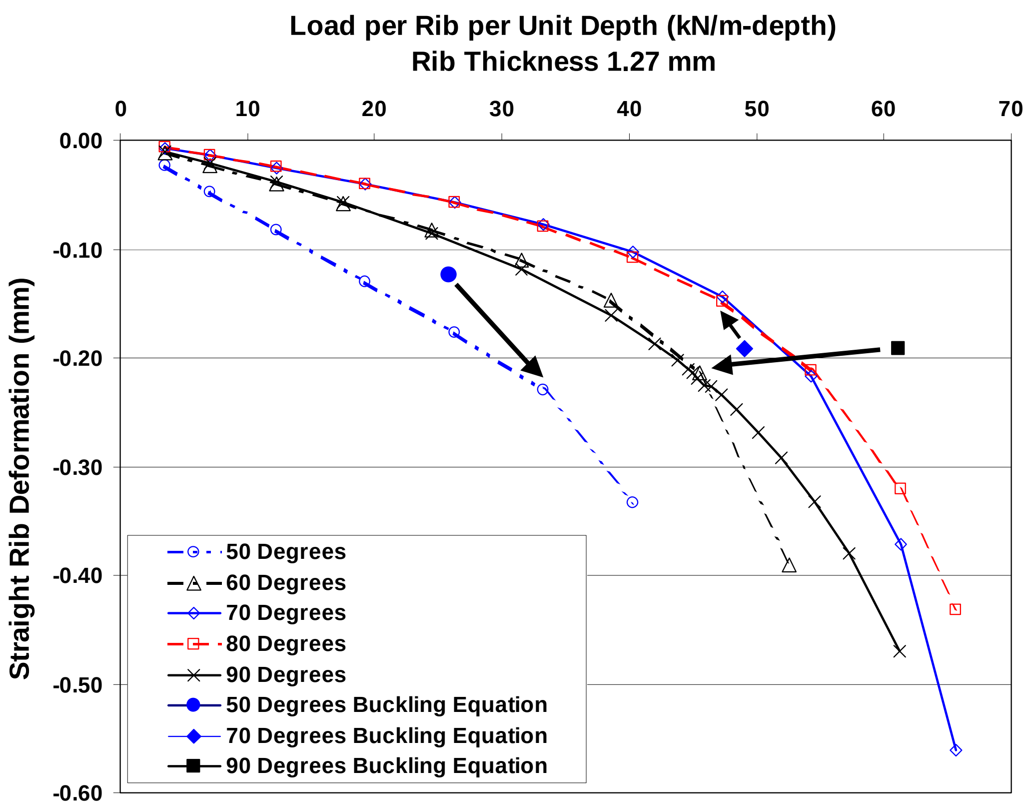

Figure 12 **Straight rib section deformation for the 3D engineered fiberboard with a rib thickness of 1.27 mm. Buckling is evident based on the departure from a linear deformation curve. Results from the buckling equation are also plotted with corresponding arrows point to approximate values where FEA predicts buckling.**

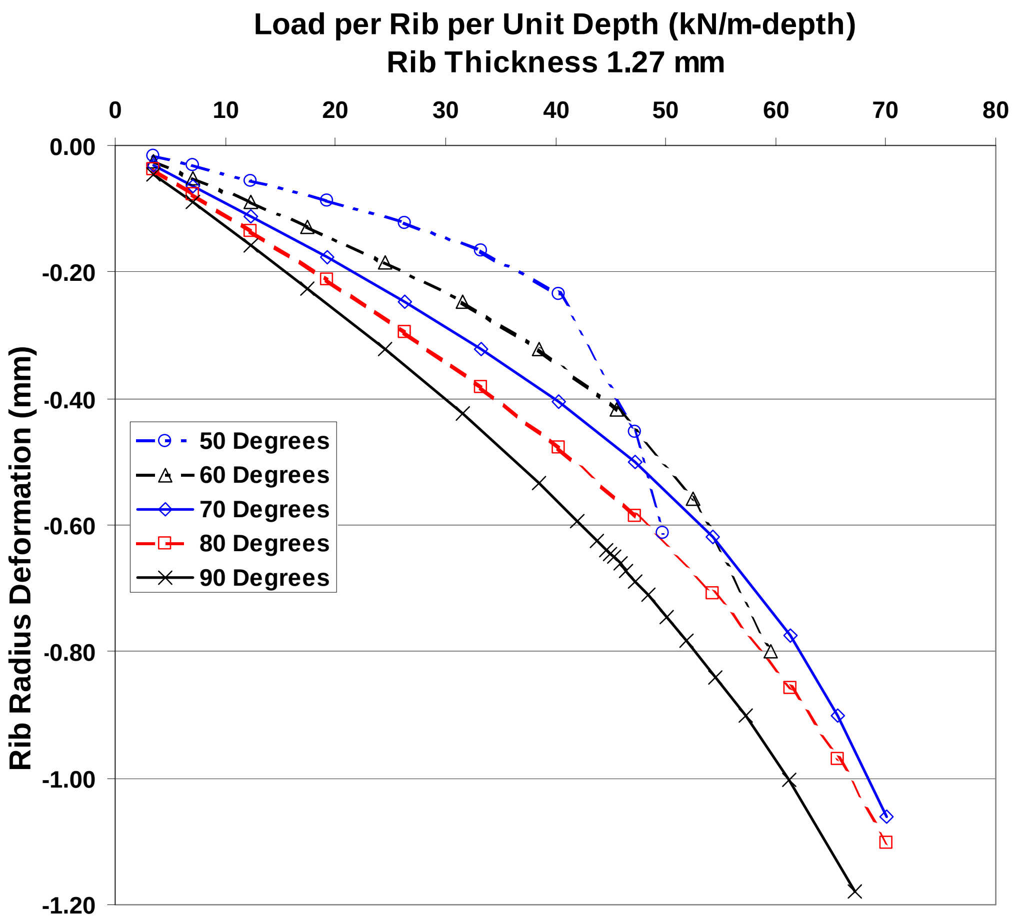

Figure 13 **Radius rib sections deformation for the 3D engineered fiberboard with a rib thickness of 1.27 mm. Buckling of the curved section at 50 degrees is evident based on the departure from a linear deformation curve.**

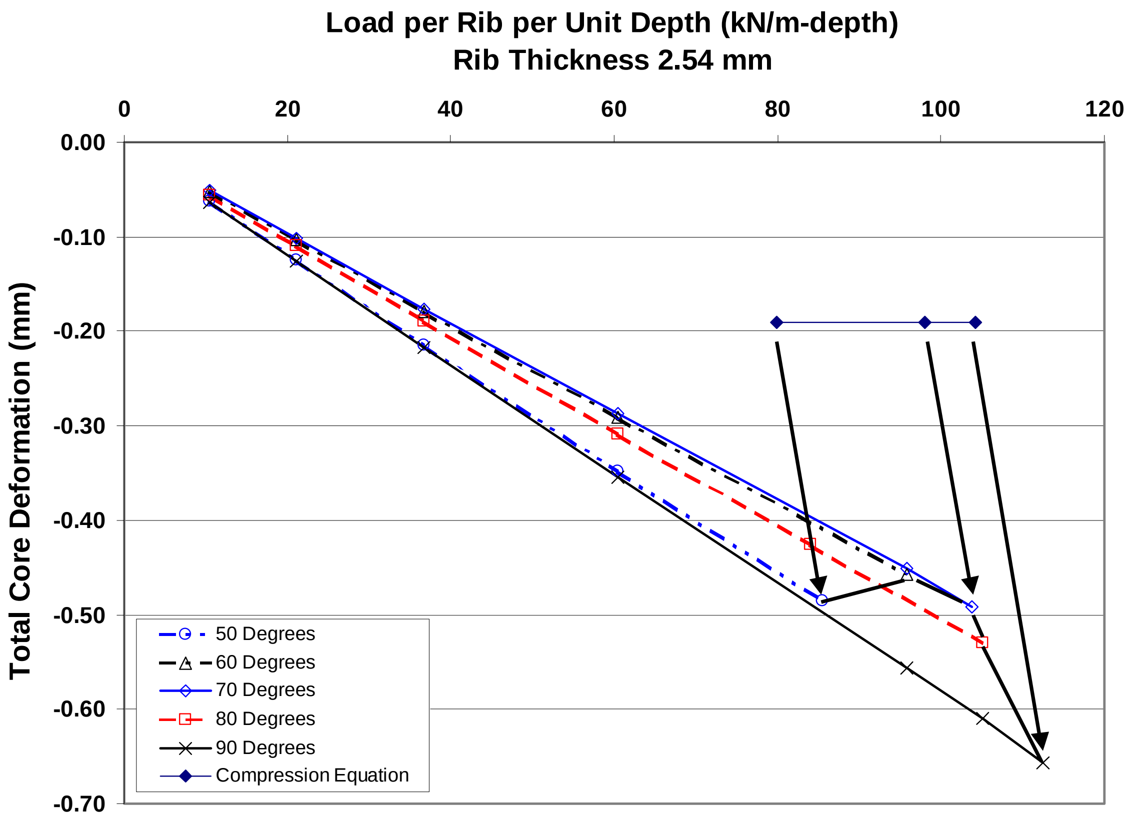

Figure 14 **Total flat-wise compression for the 3D engineered fiberboard with a rib thickness of 2.54 mm (0.1 inch). Near linear deformation response. Results from the deformation equation are also plotted with arrows pointing to approximate values where FEA predicts maximum compression stress.**

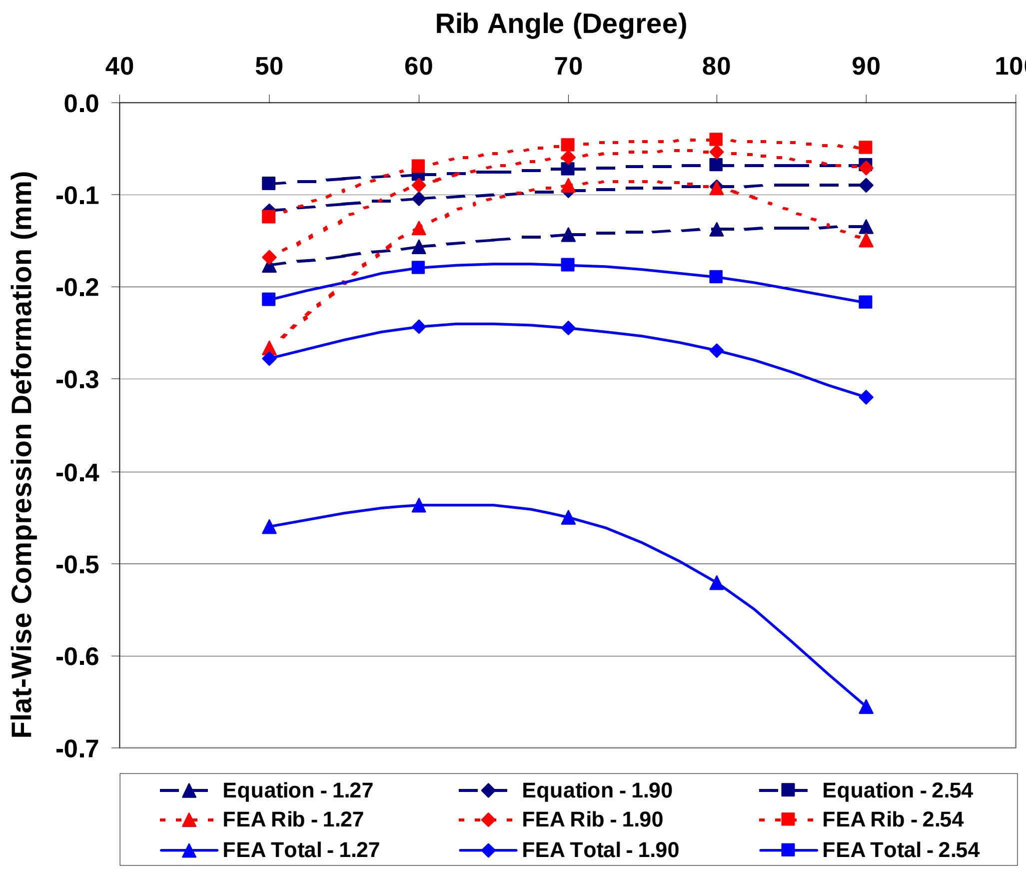

Figure 15 **Predicted flat-wise compression deformation values at 37 kN/(m-depth) (210 lbs/in-depth) load for the 3 rib thicknesses, 1.27 mm, 1.90 mm, and 2.54 mm obtained from: 1. simplified equations of deformation; 2. FEA for the straight rib section of the core only; and 3. FEA total deformation of the core.**